THE JOURNAL OF PHYSICAL CHEMISTRY C

Article

pubs.acs.org/JPCC

Solid-State Dye-Sensitized Solar Cells using Ordered TiO_2 Nanorods on Transparent Conductive Oxide as Photoanodes

Mingkui Wang,[†,‡] Jie Bai,[†] Florian Le Formal,[‡] Soo-Jin Moon,[‡] Lê Cevey-Ha,[‡] Robin Humphry-Baker,[‡] Carole Grätzel,[‡] Shaik M. Zakeeruddin,*[,‡] and Michael Grätzel*[,‡]

[†]Michael Grätzel Center for Mesoscopic Solar Cells, Wuhan National Laboratory for Optoelectronics, Huazhong University of Science and Technology, 1037 Luoyu Road, 430074 Wuhan, P. R. China

[‡]Laboratory for Photonics and Interfaces, Institute of Chemical Sciences and Engineering, Swiss Federal Institute of Technology, CH 1015 Lausanne, Switzerland

ABSTRACT: TiO_2 nanorod arrays were prepared on top of a transparent conductive glass substrate covered with a thin TiO_2 compact layer. Solid-state dye-sensitized solar cells (SSDSCs) were fabricated using these structured TiO_2 films sensitized with C106 dye as a photoanode and 2,2′,7,7′-tetrakis-(*N*,*N*-dipmethoxyphenylamine) 9,9′-spirobifluorene (spiro-MeOTAD) as the organic hole-transporting material. Photovoltaic power conversion efficiency of 2.9% was obtained at full sunlight intensity. The electron lifetime as well as the electron diffusion coefficient in the device was determined by charge extraction, transient photovoltage decay, and open-circuit photovoltage decay experiments.

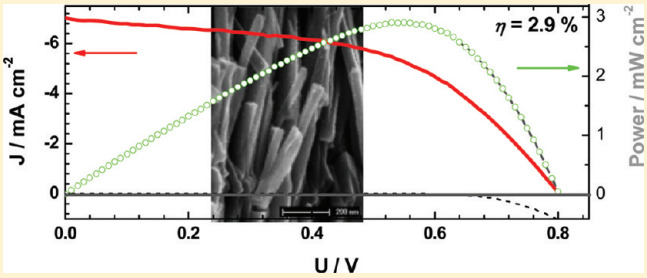

1. INTRODUCTION

Solar energy devices have been the focus of many groups as an alternative to nonrenewable power sources, providing solutions to environmental and ecological problems concomitant with these technologies.[1] Dye-sensitized solar cells (DSCs) based on organic materials and nanoparticle hybrid technologies are currently attracting widespread attention because of their potential low cost and power conversion efficiencies of over 11%,[2−5] rendering them one of the most promising future PV technologies. In the DSC, light is absorbed by a monolayer of dye located at the interface between a transparent oxide electron conductor and hole transporting material (HTM). The effective surface area for dye adsorption can be greatly enhanced with a mesoporous film consisting of TiO_2 nanoparticles. Upon illumination, the photoexcited dye injects an electron into the conduction band of the TiO_2. The injected electrons then migrate through the TiO_2 network to be collected at the transparent electrode substrate. The oxidized dye is subsequently regenerated through the electrolyte, generally containing iodide/tri-iodide as a redox couple.

Replacement of the liquid electrolyte in these devices by a solid-state charge carrier material helps to avoid encapsulation problems. Bach et al. were the first to demonstrate a solid-state DSC (SSDSC) utilizing an organic, HTM, i.e., (2,2′,7,7′-tetrakis-(*N*,*N*-dipmethoxyphenylamine) 9,9′-spirobifluorene coded spiro-MeOTAD to replace the liquid electrolyte.[6] Generally, in the fabrication of SSDSC, a thin photoanode (1.5 to 3 μm) consisting of colloidal TiO_2 nanoparticles has been used to realize mesoporous layer. Using this device structure, SSDSCs showing high efficiencies have been reported employing an amphiphilic heteroleptic ruthenium sensitizer (∼5%) and D-π-A organic dye (∼6%).[7−9]

Electrodes made from one-dimensional oxides such as nanowires, nanorods, and nanotubes have been proposed for improving the charge collection efficiency of ordered-bulk-heterojunction devices and DSCs.[10−12] These structured materials have been prepared by using anodic oxidation, electrochemical lithography, photoelectrochemical etching, sol−gel processing, hydrothermal synthesis, and template synthesis.[13−19] Several groups have shown that ordered TiO_2 structures may enhance DSC's power conversion efficiencies.[20] For example, Grimes and co-workers have recently reported a 6.9% efficient liquid-based device prepared by a titania nanotube array film grown on transparent conducting glass.[21] While many of these studies have focused on the direct anodization of titanium metal, other preparation techniques such as solution phase growth of nanotubes have also shown much promise.[22]

Recently, we reported SSDSCs using highly ordered, vertically oriented TiO_2 nanotube arrays as the anodes, which had been prepared by potentiostatic anodization of titanium on the FTO-coated glass substrate, yielding a power conversion efficiency of 1.67% when measured under full sunlight intensity.[23] However, the anodization procedure risks destroying the compact blocking layer, which prevents shorting of the device by direct contact between the hole-conductor (spiro-MeOTAD) and the highly doped SnO_2 layer on the glass. It is

Received: September 21, 2011
Revised: January 6, 2012
Published: January 9, 2012

   dx.doi.org/10.1021/jp209130x | *J. Phys. Chem. C* 2012, 116, 3266−3273

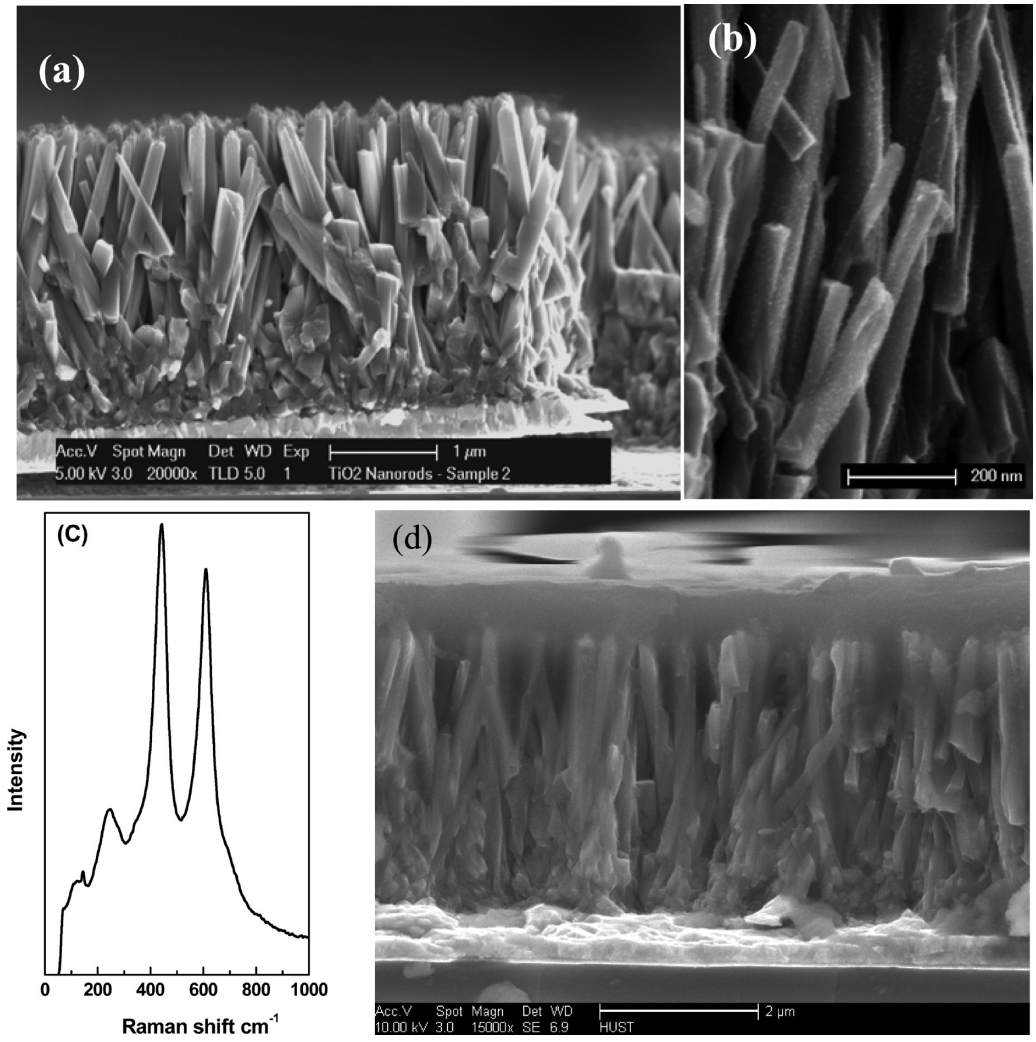

Figure 1. SEM images in cross-sectional view of oriented rutile TiO_2 nanorod film grown on compact TiO_2 layer covered FTO substrate in a 30 mL solution of deionized water, 30 mL of hydrochloric acid, and 1 mL of titanium isopropoxide at 180 °C for 5 h before (a) and after (b) $TiCl_4$ treatment. (c) Raman spectroscopy of the sample at 180 °C for 5 h. (d) Cross-sectional scanning electron micrograph of the nanorod photoanode after spiro-MeOTAD infiltration by spin coating.

important to develop a suitable method for preparation of the one-dimensional (1-D) electrodes for SSDSCs. In fact, fabricating highly ordered 1-D nanostructures directly onto a transparent conductive oxide substrate for front side illuminated DSCs has been one of the most challenging tasks in this domain.[24] Liu et al. have reported a 3.0% efficient volatile electrolyte-based DSC fabricated by vertically aligned single-crystal rutile TiO_2 nanowires (prepared by the hydrothermal method) on transparent conductive fluorine doped tin oxide (FTO) substrates.[25] Preliminary results obtained with these TiO_2 nanorods are promising for the development of solid-state DSCs.

2. RESULTS AND DISCUSSION

Figure 1 shows typical SEM images of the TiO_2 nanorod film grown at 180 °C for 5 h. The images at different locations and magnifications reveal that the entire surface of compact TiO_2/FTO substrate is covered uniformly with TiO_2 nanorods. The cross-sectional view in Figure 1a shows that the rod's side surface is smooth. The nanorods are tetragonal in shape with square top facets (see Figure 1b), which is the expected habit of growth for the tetragonal crystal structure, showing no difference with rods grown on the bare FTO substrate. After 5 h of growth, the average diameter and length, as determined from SEM images, were 50 ± 5 nm and 1.9 ± 0.3 μm, respectively. This result demonstrates that the presence of the TiO_2 compact layer (around 150 nm thick) does not have any influence on the growth of TiO_2 nanorods. It has been reported that the films deposited on FTO substrates by using this method are rutile TiO_2.[25] Raman spectroscopy confirms the presence of rutile phase with peaks at 144, 242, 452, and 610 cm^{-1} (Figure 1c).[26,27]

Complete solid-state DSC devices were prepared using those thin films. After treatment with a 20 mM $TiCl_4$ solution (see Experimental Section), the thin films were dipped overnight in a mixture of acetonitrile and *tert*-butyl alcohol solution of ruthenium complex dye. The thin film was then ready to be infiltrated with a solution of spiro-MeOTAD HTM. Each film was covered by a small quantity (50−70 uL) of spiro-MeOTAD solution before spin coating at 1200 rpm for 45 s in order to maximize pore filling.[28] The penetration of the HTM into the nanorod-based TiO_2 film was estimated with SEM measurements. Figure 1d presents a cross-sectional SEM of the nanorod-based photoanode after infiltration of spiro-MeO-

dx.doi.org/10.1021/jp209130x | J. Phys. Chem. C 2012, 116, 3266−3273

TAD, where it was detected at the bottom of the 2 μm thin film. A capping layer of spiro-MeOTAD of approximately 500 nm thick was observed. The filling fraction of HTM was estimated to be 78% by following the Snaith et al. procedure.[29] Similar results were obtained on a 20 nm sized colloidal TiO_2 film[28,30] and three-dimensional (3-D) fibrous network of fused single-crystalline anatase nanowires[31] films used for high-efficiency solid-state DSCs.

The representative current−voltage (J−V) curves for devices using different length titania nanorod films as anodes (rod lengths in device **A**, 2.0 μm, black; device **B**, 2.7 μm, red; device **C**, 3.7 μm, blue) are shown in Figure 2a (left ordinate). Upon

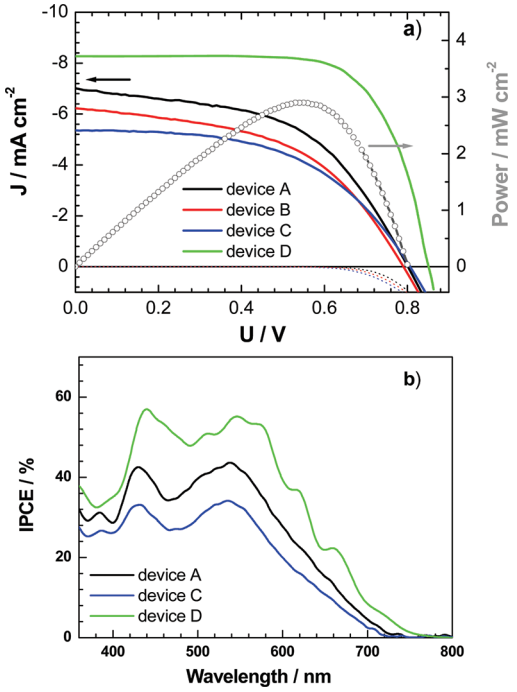

Figure 2. (a) J−V curves of SSDSC utilizing a TiO_2 nanorod-based anode of varying rod length: device **A**, 2.1 μm, device **B**, 2.68 μm, and device **C**, 3.65 μm, comparing to device **D** containing nanoparticle-based TiO2 films with the thickness of 1.9 μm under full sunlight intensity (light intensity: 100 mW cm $^{-2}$, AM 1.5 sunlight). (b) The photocurrent action spectrum of different SSDSCs devices (**A**, **C**, and **D**).

illumination under AM1.5G conditions (Oriel 450 W solar simulator, 100 mW/cm^2), device **A** exhibited an open-circuit voltage (V_{oc}) of 0.802 V, a short-circuit current density (J_{sc}) of 7.01 mA/cm^2, and a fill factor (FF) of 0.52, giving an overall power conversion efficiency (η) of 2.9% (Figure 2a, right ordinate). The right ordinate scale refers to the open-circled line, illustrating the voltage dependence of the power density of device **A**. The photovoltaic parameters, i.e., the open circuit voltage (V_{oc}), fill factor (FF), short circuit current density (J_{sc}), and the photovoltaic conversion efficiency (η) for devices **A**, **B**, and **C** are tabulated in Table 1. The nanorod film array-based photoanodes (devices A, B, C) using the organic solid-state HTM show comparable performance (2.3% < η < 3.0%) to a volatile electrolyte-based DSC employing a similar photoanode structure (η = 3.0%).[25] We note that the J_{sc} decreased as a function of increasing nanorod length most likely due to the formation of the denser bottom edge of the film due to longer growth time and a reasonably small increase in the dark current.

Table 1. Performance [Short Circuit Photocurrent Densities (J_{sc}), Open-Circuit Voltage (V_{oc}), Fill Factor (FF) and Efficiency (η)] of the SSDSCs Sensitized with C106 Dye with Different Photoanodes

device	V_{oc} (mV)	J_{sc} (mA cm^{-2})	FF	efficiency (%)	Absorbance at 550 nm (Q. D.)
A[a]	802	7.011	0.52	2.92	0.24
B[b]	791	6.226	0.50	2.42	
C[c]	807	5.358	0.53	2.25	
D[d]	848	8.27	0.71	4.99	0.45

[a]Device **A** using the nanorod TiO_2-based films with the length of 2.0 μm, which were made at 180 °C for 5 h. [b]Device **B** using the nanorod TiO_2-based films with the length of 2.68 μm, which were made at 180 °C for 7 h. [c]Device **C** using the nanorod TiO_2-based films with the length of 3.68 μm, which were made at 150 °C for 20 h. [d]Device **D** using the homemade colloidal nanoparticle-based TiO_2 films with the thickness of 1.9 μm.

Under similar conditions, the photovoltaic parameters of a standard SSDSC (device D in Table 1) utilizing a mesoporous titania electrode fabricated from 20 nm colloidal particulate TiO_2 were V_{oc} = 848 mV, J_{sc} = 8.27 mA/cm^2, and FF = 0.71, yielding a certified photovoltaic conversion efficiency of 5.0%.[32]

The incident photon-to-current conversion efficiency (IPCE) spectrum for device **A** exceeds 40% over the spectral range of 500 to 560 nm reaching a maximum of approximately 44% at 540 nm (see Figure 2b). The IPCE of device **D** reaches a maximum of 55% at 540 nm.[32] The lower photocurrents observed in SSDSC devices utilizing the nanorod films correlated with a decrease in the amount of adsorbed dye. As indicated by the SEM images (Figure 1), the average dimensions of the rod-shaped rutile rods (50 nm diameter) are larger than that of the spherically shaped antase particles (20 nm diameter), implying that the particle density and thus internal surface area of the nanorod-based film, is smaller than that of the colloidal nanoparticle-based film. This suggests that the difference in the short-circuit photocurrent between nanorod and nanoparticle-based SSDSC cells (Table 1) could be due to their surface area (i.e., the amount of dye adsorbed). Absorbance measured at 550 nm as shown in Table 1 demonstrates a lower optical density of the dye-sensitized nanorod-based TiO_2 film (~0.2) compared to the dye coated onto colloidal nanoparticles (~0.45). This result is consistent with the previous reports on the comparison of dye-sensitized rutile- and anatase-based TiO_2 solar cells.[13,19]

To understand the differences in the photovoltaic performance of nanorod-based SSDSCs compared to colloidal nanoparticle-based devices, the electron recombination kinetics of these two types of photoanodes were investigated by monitoring the V_{oc} decay as a function of time upon tuning off the illumination.[33] It is evident in Figure 3a that the DSC based on nanorod photoanode TiO_2 (red, device **A**) has a significantly slower V_{oc} decay rate than those based on the TiO_2 colloidal nanoparticles (green, device **D**). The kinetics of electron transfer to the oxidized HTM is usually discussed in terms of the apparent charge recombination lifetime, τ_n. From the V_{oc} decay rate, the apparent recombination of photogenerated electrons (τ_n), denoting the length of time photogenerated electrons remain in the film before recombining, can be evaluated by the following expression:[33]

dx.doi.org/10.1021/jp209130x | J. Phys. Chem. C 2012, 116, 3266−3273

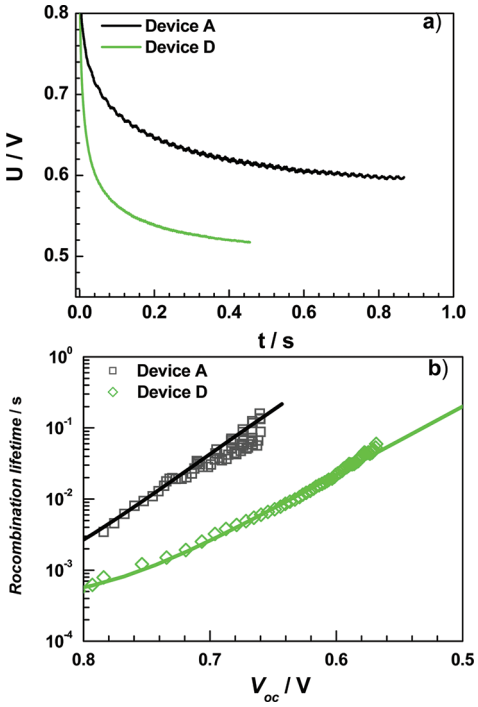

Figure 3. (a) Comparative open circuit voltage decay, V_{oc} of SSDSC devices based on a TiO_2 nanorod array (**A**) and TiO_2 colloidal photoanodes (**D**): device **A**, 2.0 μm length thickness TiO_2 nanorods; and device **D**, 1.9 μm length thickness TiO_2 colloidal nanoparticles. (b) The electron recombination lifetime derived from eq 1 as a function of V_{oc}. The solid lines are the fitting results.

$$\tau_n = -\frac{k_B T}{e}\left(\frac{dV}{dt}\right)^{-1} \quad (1)$$

where k_B is the Boltzmann constant, and T is the temperature. According to the quasi-static treatment, the apparent charge recombination lifetime (τ_n) under different energy levels is related to the conduction-band electron lifetime (τ_e) by using the following expression, denoting the length of time photogenerated electrons remain in the film before recombining:

$$\tau_n = \tau_e\left(1 + \frac{\partial n_t}{\partial n_c}\right) \quad (2)$$

where n_t is the trapped electron density, τ_e is the inverse of the pseudo first-order rate constant for the back transfer of electrons from the conduction band, and n_c is the conduction band electron density.

The calculated apparent charge recombination lifetime τ_n was plotted as a function of V_{oc} in Figure 3b for the two types of photoanodes. It is observed that at identical V_{oc}, the apparent charge recombination lifetime τ_n values found for the TiO_2 nanorod-based anode (red, device **A**) is longer than those of TiO_2 nanoparticle-based anodes (green, device **D**) by more than an order of magnitude. It implies that the conduction band electron lifetime (τ_e) is longer for the nanorod-based anode (see eq 2).[39] This result has been observed for DSC devices using a 1-D structured photoanode, including nanotubes and nanorods.[34,35] The trend of the calculated charge recombination lifetime of these devices compared at identical V_{oc} is contrary to the above measured photocurrent densities and photovoltages (see Table 1). In general, longer conduction-band electron lifetime (τ_e) should bring better photovoltaic performance of DSCs, such as an enhanced photovoltage.[36] In order to explain the much longer apparent charge recombination lifetime τ_n of the TiO_2 nanorod-based SSDSC compared to the TiO_2 nanoparticle-based SSDSC, Enache-Pommer et al. suggested that an internal radial electrical field was developed within the nanorods.[35]

The photovoltage of a DSC device is approximately equal to the energy difference of nanocrystalline TiO_2 Fermi level and to that of the HTM. Note that the Fermi level is a hypothetical level of potential energy for an electron inside a crystalline solid. Thus, at the open circuit condition, the recombination dynamics between the injected electrons with the oxidized states of HTM defines the open circuit voltage.[36−38] Under illumination, electron injection from the dye increases the electron density n_t in the mesoporous TiO_2 film, which in turn raises the quasi-Fermi level, E_F, by an amount corresponding to the photovoltage V_{oc}. At the V_{oc}, the rate of light-induced electron accumulation in the photoanode equals that of charge recombination with the oxidized form of the redox couple.[37,38] We can suspect that two films having different electron concentrations may give the same V_{oc} if the difference in electron concentration is compensated by a change in the rate constant for charge recombination. According to the relationship between the carrier densities and Fermi energies, the increased electron density raises the Fermi level of the TiO_2 photoanode.[39] Presumably having the same Fermi level in the HTM among the TiO_2 nanorod-based and nanoparticle-based SSDSC due to the same HTM and fabrication process. In order to compare the apparent charge recombination lifetimes, it is therefore preferable to plot the recombination lifetime vs the charge density, not the V_{oc}.[38] The rate of the overall electron transfer process may be written formally in terms of the concentrations of reactants (n_t and [Ox]) and the corresponding reaction orders γ and β.[37]

$$-\frac{dn}{dt} = k{n_t}^{\gamma}[Ox]^{\beta} \quad (3)$$

where n is the number of free electrons, and k is the rate constant. If the electron is first order in n_t and the [Ox] is effectively constant, the conduction-band electron lifetime, (τ_e), can be defined as

$$\tau_e = \frac{1}{k_{et}[Ox]^{\beta}} \quad (4)$$

Thus,

$$\frac{dn}{dt} = -n(\tau_e)^{-1} \quad (5)$$

$$\tau_e = -n_t\left(\frac{dn}{dt}\right)^{-1} \quad (6)$$

Note that in eq 3, we can introduce the V_{oc} by

$$\frac{dn}{dt} = \frac{dn}{dV_{oc}}\frac{dV_{oc}}{dt} \quad (7)$$

Therefore, from eqs 5 and 6, one can find the relationship between the conduction-band electron lifetime τ_e and V_{oc}

$$\tau_e = -n_t\left(\frac{dn}{dt}\right)^{-1} = -n_t\frac{dV_{oc}}{dn}\frac{dt}{dV_{oc}} \quad (8)$$

dx.doi.org/10.1021/jp209130x | J. Phys. Chem. C 2012, 116, 3266−3273

Thus, eq 8 can be satisfied with the results from the charge extraction method and the voltage decay techniques, which are described in the Experimental Section.

There are several approaches available for deriving the electron density and the apparent recombination electron lifetime, including transient laser spectroscopy, electrochemical impedance spectroscopy, and transient photovoltage decay.[39−42] In this study, transient photovoltage decay measurements were used to derive the charge recombination kinetics in the solid-state DSC devices.[43,44] Figure 4a exhibits

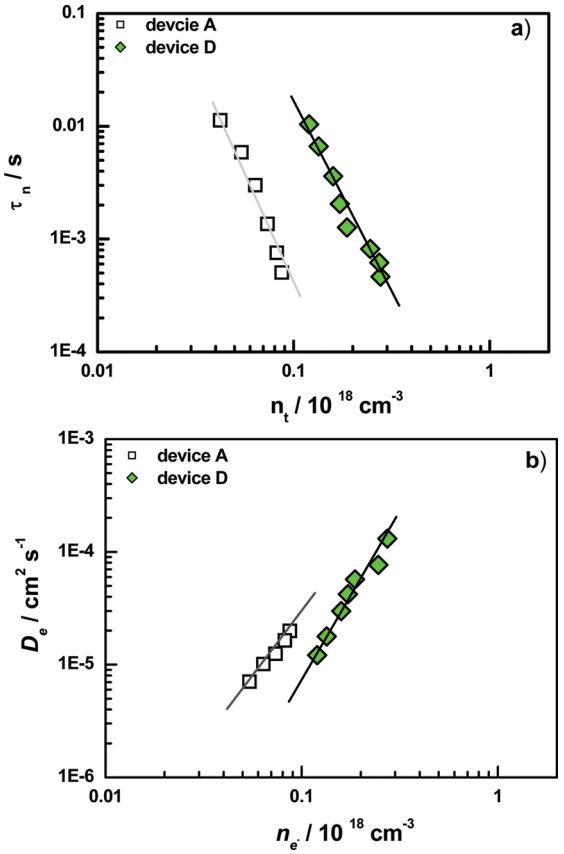

Figure 4. (a) Charge recombination lifetime (τ_n) and (b) electron diffusion coefficients of SSDSC devices: black, device **A**, 2.0 μm thick of TiO_2 nanorod-based anode; and green, device **D**, 1.9 μm thick of TiO_2 colloidal nanoparticle-based anode. The abscissa indicates the extracted charge density under the same intensity as used for the transient photovoltage measurements.

the apparent charge recombination lifetime measurements, performed at open circuit, as a function of the extracted charge density, n_t (where $n_t = \Delta Q/(A_r d/(1-p))$ and ΔQ equals the extracted charge, A_r is the real interface area of the photoanode, d is related to the film thickness of the photoanode, and p represents the porosity of the anode).

To get the comparative analysis, the term f_r, the roughness factor, is introduced,[45] where $f_r = A_r/A_g$ with A_g corresponding to the geometrical surface area. The relationship between the roughness factor (f_r) and the porosity (p) of the thin film with nanostructures has been determined to be $f_r = (1-p)\rho A$, where ρ is the TiO_2 density (3.895 g cm^{-3} for anatase type TiO_2; 4.2743 g cm^{-3} for rutile type TiO_2), and A is the specific surface area (in the unit of cm^2 g^{-1}) determined by BET measurement. The roughness factor of the 2 μm thick TiO_2 nanoparticle (20 nm sized) film, typically around 270,[46] is larger than that of nanorod array electrode, which is estimated to be approximately 22 (with the diameter of 50 nm and length of 2 μm, the area density of 50 rods/ μm^2). Using this factor, we can accurately compare the apparent recombination electron lifetime (under identical charge density, Figure 4a) or the effective electron diffusion coefficient (Figure 4b) of device **A** to that of device **D** under a normalized charge density. The linear fitting of all the data (in logarithmic scale, Figure 4a) arises a similar slope value ($\sim -4 \pm 0.5$) for both devices **A** and **D**, indicative of the prevalence of an identical recombination mechanism in both devices. At identical charge density, the apparent recombination lifetime in the nanorod array and colloidal nanoparticle devices exhibits noticeable differences, underlining that recombination kinetics are more facile on the nanorod/HTM interface as compared to that on the colloidal nanoparticle/HTM heterojunction. A higher open circuit voltage for the SSDSC devices utilizing colloidal nanoparticle-based anodes is thus expected as confirmed experimentally. The significant finding demonstrates that an enhanced recombination dynamics is obtained using the nanorod array geometry, being consistent with the device photovoltaic measurements, which also can be attributed to more significant recombination or back reaction of the injection electrons for rutile surfaces.[13,19]

Figure 4b presents the comparative effective electron diffusion coefficient D_n of the two devices (**A** + **D**) vs the charge density. It is generally accepted that the transport of electrons though a nanostructured film is slowed by multiple trapping events, principally involving surface states.[38] As illustrated in Figure 4b, D_n for device **A** is slightly higher than that of device **D**, due to less interparticle connections in an oriented architecture.[20,42] Thus, the effective electron diffusion length L_e ($L_e = (D_e\tau_e)^{1/2}/d$, d being the film thickness) in these devices can be calculated to be ~1.1 and 3.5 μm for the devices using nanorods or nanocolloids at a charge density of 1.0×10^{17} cm^{-3}, respectively. The charge collection efficiency η_{cc} ($\eta_{cc} = (L_e)/d[1 - \exp(-d/L_e)]$) can be estimated to be 0.66 and 0.87, respectively. A longer electron diffusion length guarantees a more highly efficient electron collection. Thus, the longer apparent charge recombination lifetime and greater electron diffusion length at the identical charge density in the nanocolloid-based devices are both responsible for the observed higher V_{oc} and J_{sc} valves. Furthermore, the IPCE value at 540 nm ($IPCE_{(\lambda)} = LHE_{(\lambda)}\phi_{inj}\eta_{cc}$, $LHE_{(\lambda)}$ being the light harvesting efficiency for photons of wavelength λ ($LHE_{(\lambda)} = 1 - 10^{-A}{}_{(\lambda)}$), and ϕ_{inj} being the quantum yield for electron injection from the excited sensitizer in the conduction band of the semiconductor oxide) of SSDSCs could be evaluated to be 0.2 and 0.53 for the nanorod- and nanocolloid-based devices, respectively, by using the adsorption A and assuming that ϕ_{inj} equals 1. The measured IPCE value of a nanorod-based device at that wavelength (Figure 2b) was larger than that of the calculated value (about 0.4 vs 0.2), which could be attributed to the scattering effect of nanorods with a large particle size.

A comparison of the chemical capacitance of the devices using nanorod and nanoparticle films is illustrated in Figure 5. The capacitance of the TiO_2/electrolyte interface at the V_{oc} can be calculated as $C_\mu = \Delta Q/\Delta V$, where ΔV is the peak of the transient photovoltage decay, and ΔQ is the number of electrons injected during the red light flash (see Experimental Section). The latter is obtained by integrating a short-circuit photocurrent transient generated from an identical red-light

dx.doi.org/10.1021/jp209130x | J. Phys. Chem. C 2012, 116, 3266−3273

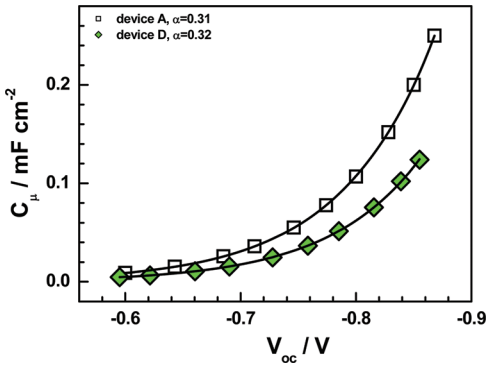

Figure 5. Chemical capacitance values of SSDSC (devices fabricated with 2.0 um thick nanorod array-based (**A**) and a colloidal TiO_2-based (**D**)) generated from transient photovoltage decay and photocurrent decay measurements.

pulse. As presented in Figure 5, the capacitance for both TiO_2 photoanodes increases exponentially with forward bias. A parameter α ($\alpha = T/(T_0)$, T_0 being a parameter characteristic with temperature units that indicates the depth of the distribution) can be obtained by fitting the experimental data, which describes the trapping states distribution.[39] A small α value corresponds to a broader distribution of traps. The α values of devices **A** and **D**, respectively, were found to be 0.31 and 0.32, indicating that the electronic state distribution remains constant for both devices. Device **D** exhibits a smaller capacitance than device **A** measured under the same conditions. A major part of this difference arises from a shift of the conduction band edge. It is well-known that the rutile structure of TiO_2 has a lower conduction band (0.1−0.2 eV) energy than that of the anatase crystal structure.[47] The method applied for charge collection under short circuit conditions may underestimate the actual injected electrons by the fraction that is lost due to recombination during transport. This error can be larger in the solid-state device, but it will affect only the magnitude, but not on the shape of the calculated capacitance and charge density. Note that the values of charge density from the charge collection, interpretation of charge density, and chemical capacitance in the films are not straightforward. The physical interpretation of these numbers must be carried out with caution, keeping in mind the assumptions used in deriving them.

3. CONCLUSIONS

In summary, we have synthesized vertically aligned TiO_2 nanorod arrays directly on top of a compact TiO_2 layer, which has been deposited onto TCO, and used them in the fabrication of SSDSCs, achieving an efficiency of 2.9% under 100 mW/cm^2 simulated sunlight. When compared to the state-of-art SSDSC cells based on sintered TiO_2 nanoparticles, our current TiO_2 nanorod-based SSDSC have a lower efficiency due to their significantly smaller roughness factor and consequently lower light harvesting. Detailed studies showed that at identical charge density, the apparent recombination lifetime of photogenerated electrons in TiO_2 nanorods is shorter than that observed in sintered TiO_2 nanoparticles, thus a lower photovoltaic performance.

4. EXPERIMENTAL SECTION

4.1. Preparation of TiO_2 Nanorods on Transparent Substrates. In the present work, TiO_2 nanorods were synthesized with a previous reported procedure.[24] Typically, 30 mL of deionized water was mixed with 30 mL of concentrated hydrochloric acid (38% by weight) by stirring. After cooling down to room temperature, 1 mL of titanium isopropoxide (99% Aldrich) was added into this mixture and stirred for 5 min. Then, the solution was transferred in a Teflon-lined stainless steel autoclave (125 mL volume, Parr Instrument Co.). A spray pyrolysis technique was used to coat the SnO_2/F conducting glass substrates (Tek, 15 Ω/square) with a thin compact layer of TiO_2 (around 150 nm thick) by using a solution of 5 mL of titanium isopropoxide into 45 mL of ethanol and oxygen as the carrier gas. After sintering at 450 °C for 30 min in the air, the FTO glass with a TiO_2 compact layer was placed at an angle against the wall of the Teflon-line with the compact layer facing down. The hydrothermal synthesis was conducted at 150−180 °C for 5−20 h in an electric oven. After synthesis, the autoclave was cooled to room temperature under flowing water. The samples were taken out, rinsed extensively with deionized water, and allowed to dry in ambient air. The electrodes coated with the TiO_2 nanorods were gradually heated under an airflow at 325 °C for 5 min, at 375 °C for 5 min, and at 450 °C for 15 min and, finally, at 500 °C for 15 min. The TiO_2 nanorod film thus produced was treated with a 20 mM $TiCl_4$ solution at room temperature for 14 h, then rinsed with water completely and sintered at 450 °C in the air for 30 min.

4.2. Device Fabrication. Solar cell fabrication and characterization was performed as previously described.[32,39] Before dye dipping, the TiO_2 electrodes were heated with hot airflow at 500 °C for 30 min, after cooling to 80 °C, the TiO_2 electrode was immersed into a 0.3 mM C106 dye[4b] solution in a mixture of acetonitrile and *tert*-butyl alcohol (volume ratio, 1:1) and kept at room temperature for 14−16 h to ensure complete sensitizer uptake. After rinsed with acetronile in the dry air atmosphere, the dye-sensitized TiO_2 substrates were covered by solid-state hole conductor matrix by spin-coating of a spiro-MeOTAD solution. The spiro-MeOTAD solution (0.17 M in chlorobenzene) contains final concentrations of 0.11 mM *tert*-butylpyridine and 0.21 mM $Li[CF_3SO_2]_2N$ (added from highly concentrated acetonitrile solutions). Finally, a gold contact (100 nm) was deposited on the organic semiconductor film by evaporation (EDWARDS AUTO 500 Magnetron Sputtering System).

4.3. Photovoltaic Characterization. A 450 W xenon light source (Oriel, USA) was used to give an irradiance of 100 mW cm^{-2} (the equivalent of one sun at air mass (AM, 1.5) at the surface of solar cells. The spectral output of the lamp was matched in the region of 350−750 nm with the aid of a Schott K113 Tempax sunlight filter (Präzisions Glas & Optik GmbH, Germany) so as to reduce the mismatch between the simulated and true solar spectra to less than 2%. The current−voltage characteristics of the cell were obtained by applying external potential bias to the cell and measuring the generated photocurrent with a Keithley model 2400 digital source meter (Keithley, USA). A similar data acquisition system was used to control the incident photon-to-collected electron conversion efficiency measurement. Under computer control, light from a 300 W xenon lamp (ILC Technology, U.S.A.) was focused through a Gemini-180 double monochromator (Jobin Yvon Ltd., U.K.) onto the photovoltaic cell under test. The monochromator was incremented through the visible spectrum to generate the *IPCE* (λ).

dx.doi.org/10.1021/jp209130x | *J. Phys. Chem. C* 2012, 116, 3266−3273

4.4. Determination of Apparent Recombination Electron Lifetime, Electron Diffusion Coefficients and the Density of Electrons in the Titania Film by Transient Photovoltage Decay and Charge Extraction Measurements. For the transient photovoltage decay measurements, a white light bias on the solid-state DSC sample was generated from an array of diodes. Red light pulse diodes (0.05 s square pulse width, 100 ns rise and fall time) controlled by a fast solid-state switch were used as the perturbation source. The voltage dynamics were recorded on a PC-interfaced Keithley 2400 source meter with a 500 μs response time. The perturbation light source was set to a suitably low level in order for the voltage decay kinetics to be monoexponential. By varying the white light bias intensity, the recombination rate constant and electron diffusion rate constant could be estimated over a range of applied biases. Before the LEDs switched to the next light intensity, a charge extraction routine was executed to measure the electron density in the film. In the charge extraction techniques, the LED illumination source was turned off in <1 μs, while simultaneously, the cell was switched from open to short circuit. The resulting current, as the cell returns to $V = 0$ and $J = 0$, was integrated to give a direct measurement of the excess charge in the film at that V_{oc}, which is the minimum level of charge in the semiconducting photoanode.

4.5. Determination of Apparent Recombination Electron Lifetime in Solid-State DSC by Open-Circuit Voltage Decay (OCVD) Measurements. For the decay measurements, the cell was illuminated under with LED light source (1.5 sun light intensity) to a steady voltage. The illumination was turned off with a shutter. The OCVD was recorded by an Ecochemie potentiostat equipped with a short-interval sampling module. Typically, the measurement interval was 10 ± 50 ms.

The sample morphology was characterized using scanning electron microscopy (FEI XLF30 SFEG).

AUTHOR INFORMATION

Corresponding Author

*E-mail: shaik.zakeer@epfl.ch (S.M.Z.); michael.graetzel@epfl.ch (M.G.).

ACKNOWLEDGMENTS

We thank the Swiss National Science Foundation for financial support. M.W. thanks the National Basic Research Program of China (973 Program, No. 2011CBA00703), the National Natural Science Foundation of China (No. 20903030 and 201173091), the Chinese Ministry of Education with the Program of New Century Excellent Talents in University (NCET-10-0416), and the "Talents Recruitment Program" of HUST, the Fundamental Research Funds for the Central Universities (HUST: 2011TS021) for financial support. We thank Professor Peng Wang for providing us a sample of the C106 dye as a gift. J.B. thanks the Analytical and Testing Center at the HUST for performing SEMs of TiO_2 NRs.

REFERENCES

(1) Shah, A.; Torres, P.; Tscharner, R.; Wyrsch, N.; Keppner, H. *Science* **1999**, *285*, 692−698.

(2) Nazeeruddin, M.; De Angelis, F.; Fantacci, S.; Selloni, A.; Viscardi, G.; Liska, P.; Ito, S.; Takeru, B.; Grätzel, M. *J. Am. Chem. Soc.* **2005**, *127*, 16837−16847.

(3) Chiba, Y.; Islam, A.; Watanabe, Y.; Komiya, R.; Koide, N.; Han, L. *Jpn. J. Appl. Phys.* **2006**, *45* (Part 2), L638−L640.

(4) (a) Gao, F.; Wang, Y.; Shi, D.; Zhang, J.; Wang, M.; Jing, X.; Humphry-Baker, R.; Wang, P.; Zakeeruddin, S.; Grätzel, M. *J. Am. Chem. Soc.* **2008**, *130*, 10720−10728. (b) Cao, Y.; Bai, Y.; Yu, Q.; Cheng, Y.; Liu, S.; Shi, D.; Gao, F.; Wang, P. *J. Phys. Chem. C* **2009**, *113*, 6290−6297.

(5) Chen, C.; Wang, M.; Li, J.; Pootrakulchote, N.; Alibabaei, L.; Ngoc-le, C.; Decoppet, J.; Tsai, J.; Grätzel, C.; Wu, C.; Zakeeruddin, S.; Grätzel, M. *ACS Nano* **2009**, *3*, 3103−3109.

(6) Bach, U.; Lupo, D.; Comte, P.; Moser, J.; Weissörtel, F.; Salbeck, J.; Spreitzer, H.; Grätzel, M. *Nature* **1998**, *395*, 583−585.

(7) Krüger, J.; Plass, R.; Cevey, L.; Piccirelli, M.; Grätzel, M.; Bach, U. *Appl. Phys. Lett.* **2001**, 2085−2087.

(8) Snaith, H.; Moule, A.; Klein, C.; Meerholz, K.; Friend, R.; Grätzel, M. *Nano Lett.* **2007**, *7*, 3372−3376.

(9) Cai, N.; Moon, S.; Cevey-Ha, L.; Moehl, T.; Humphry-Baker, R.; Wang, P.; Zakeeruddin, S.; Graetzel, M. *Nano Lett.* **2011**, *11*, 1452−1456.

(10) Law, M.; Green, L.; Johnson, J.; Saykally, R.; Yang, P. *Nat. Mater.* **2005**, *4*, 455−459.

(11) Baxter, J.; Walker, A.; Van Ommering, K.; Aydil, E. *Nanotechnology* **2006**, *17*, S304−S312.

(12) Peiro, A.; Ravirajan, P.; Govender, K.; Boyle, D.; O'Brien, P.; Bradley, D.; Nelson, J.; Durant, J. *J. Mater. Chem.* **2006**, *16*, 2088−2096.

(13) Gong, D.; Grimes, C.; Varghese, O. *J. Mater. Res.* **2001**, *16*, 3331−3334.

(14) Park, N.-G.; van de Lagemaat, J.; Frank, A. J. *J. Phys. Chem. B* **2000**, *104*, 8989−8994.

(15) Masuda, H.; Kanezawa, K.; Nakao, M.; Yokoo, A.; Tamamura, T.; Sugiura, T.; Minoura, H.; Nishio, K. *Adv. Mater.* **2003**, *15*, 159−161.

(16) Wijnhoven, E.; Vos, W. *Science* **1998**, *281*, 802−804.

(17) Wang, W.; Varghese, O.; Paulose, M.; Grimes, C.; Wang, Q.; Dickey, E. *J. Mater. Res.* **2004**, *19*, 417−422.

(18) Hoyer, P. *Langmuir* **1996**, *12*, 1411−1413.

(19) Lu, Y.; Choi, D.; Nelson, J.; Yang, O.; Parkinson, B. A. *J. Electrochem. Soc.* **2006**, *153*, E131−E137.

(20) Zhu, K.; Neale, N.; Miedaner, A.; Frank, A. *Nano Lett.* **2007**, *7*, 69−74.

(21) Varghese, O.; Paulose, M.; Grimes, C. *Nat. Nanotechnol.* **2009**, *4*, 592−597.

(22) Feng, X.; Shankar, K.; Varghese, O.; Paulose, M.; Latempa, T.; Grimes, C. *Nano Lett.* **2008**, *8*, 3781−3786.

(23) Chen, P.; Brillet, J.; Bala, H.; Wang, P.; Zakeeruddin, S. M.; Grätzel, M. *J. Mater. Chem.* **2009**, *30*, 5325−5328.

(24) Xu, C.; Shin, P.; Cao, L.; Wu, J.; Gao, D. *Chem. Mater.* **2010**, *22*, 143−148.

(25) Liu, B.; Aydil, E. *J. Am. Chem. Soc.* **2009**, *131*, 3985−3990.

(26) Chen, X.; Lou, Y.; Samia, A. N. S.; Burda, C.; Gole, J. L. *Adv. Funct. Mater.* **2005**, *15*, 41−49.

(27) Periyat, P.; Pillai, S.; McCormack, D.; Colreavy, J.; Hinder, S. *J. Phys. Chem. C* **2008**, *112*, 7644−7652.

(28) Ding, I.; Tétreault, N.; Brillet, J.; Hardin, B.; Smith, E.; Rosenthal, S.; Sauvage, F.; Grätzel, M.; McGehee, M. *Adv. Funct. Mater.* **2009**, *19*, 2431−2436.

(29) Snaith, H.; Humphry-Baker, R.; Chen, P.; Cesar, I.; Zakeeruddin, S.; Grätzel, M. *Nanotechnology* **2008**, *19*, 424003(1−12.

(30) Schmidt-Mende, L.; Grätzel, M. *Thin Solid Films* **2006**, *500*, 296−301.

(31) Tétreault, N.; Horváth, E.; Moehl, T.; Brillet, J.; Smajda, R.; Bungener, S.; Cai, N.; Wang, P.; Zakeeruddin, S.; Forró, L.; Magrez, A.; Grätzel, M. *ACS Nano* **2010**, *4*, 7644−7650.

(32) Wang, M.; Cevey-Ha, N.; Moon, S.; Liska, P.; Humphry-Baker, R.; Moser, J.; Grätzel, C.; Zakeeruddin, S.; Grätzel, M. *Nano Today* **2010**, *5*, 169−174.

(33) Bisquert, J.; Zaban, A.; Greenshtein, M.; Mora-Seró, I. *J. Am. Chem. Soc.* **2004**, *126*, 13550−13559.

(34) Martinson, A.; McGarrah, J.; Parpia, M.; Hupp, J. *Phys. Chem. Chem. Phys.* **2006**, *8*, 4655−4659.

(35) Enache-Pommer, E.; Liu, B.; Aydil, E. *Phys. Chem. Chem. Phys.* **2009**, *11*, 9648−9652.
(36) Huang, S.; Schlichtho1rl, G.; Nozik, A.; Grätzel, M.; Frank, A. *J. Phys. Chem. B* **1997**, *101*, 2576−2582.
(37) Peter, L. *J. Phys. Chem. C* **2007**, *111*, 6601−6612.
(38) O'Regan, B.; Walley, K.; Juozapavicius, M.; Anderson, A.; Matar, F.; Ghaddar, T.; Zakeeruddin, S.; Klein, C.; Durrant, J. *J. Am. Chem. Soc.* **2009**, *131*, 3541−3548.
(39) Wang, M.; Chen, P.; Humphry-Baker, R.; Zakeeruddin, S.; Grätzel, M. *ChemPhysChem* **2009**, *10*, 290−299.
(40) Shen, Y.; Nonomura, K.; Schlettwein, D.; Zhao, C.; Wittstock, G. *Chem.—Eur. J.* **2006**, *12*, 5832−5839.
(41) Shen, Y.; Tefashe, U.; Nonomura, K.; Loewenstein, T.; Schlettwein, D.; Wittstock, G. *Electrochim. Acta* **2009**, *55*, 458−464.
(42) Kang, S.; Choi, S.; Kang, M.; Kim, J.; Kim, H.; Hyeon, T.; Sung, Y. *Adv. Mater.* **2008**, *20*, 54−58.
(43) O'Regan, B.; Nelson, J.; Durrant, J. *Acc. Chem. Res.* **2009**, *42*, 1799−1808.
(44) Shuttle, C.; Hamilton, R.; O'Regan, B.; Nelson, J.; Durrant, J. *Proc. Natl. Acad. Sci. U.S.A.* **2010**, *107*, 16448−16452.
(45) Kopidakis, N.; Neale, N.; Zhu, K.; van de Lagemaat, J.; Frank, A. *Appl. Phys. Lett.* **2005**, *87*, 202106(1−3.
(46) Ito, S.; Liska, P.; Comte, P.; Charvet, R.; Péchy, P.; Bach, U.; Schmidt-Mende, L.; Zakeeruddin, S.; Kay, A.; Nazeeruddin, M.; Grätzel, M. *Chem. Commun.* **2005**, 4351−4353.
(47) Liu, Z.; Zhang, X.; Nishimoto, S.; Jin, M.; Tryk, D.; Murakami, T.; Fujishima, A. *Langmuir* **2007**, *23*, 10916−10919.